Exsolution in La and Ni co-doped strontium titanate: a suitable anode for running SOFCs on ammonia as alternative fuel

Jonathan Cavazzani[1,*], *Enrico* Squizzato[1], *Elena* Brusamarello[1] and *Antonella* Glisenti[1,2]

[1]Department of Chemical Science, University of Padova, Via F. Marzolo 1, 35131, Padova, Italy
[2]ICMATE - Department of Chemical Science, University of Padova, Via F. Marzolo 1, 35131, Padova, Italy

Abstract. Ammonia exhibits interesting features as fuel to feed Solid Oxide Fuel Cell. Herein, Ni and La co-doped strontium titanate was synthetized using wet chemistry route. Ni nanoparticles emerged via exsolution in reducing environment to decorate the surface. X-Ray Diffraction measurements exhibits perovskite structure was also preserved after the exsolution, as expected. H_2 – Temperature Programmed Reduction highlights the great resistance of titanates in anode operation condition. Ammonia conversion in nitrogen and hydrogen were investigated by catalytic tests. It begins to decompose at 560°C and the full yield was achieved at 720°C. Electrochemical measurements were recorded at 800°C using 10% of ammonia in Ar. They were analysed though the model of equivalent circuit and two processes were attributed. Results certify Ni exsolution strongly enhances the hydrogen oxidation and the total polarisation resistance in ammonia approaches to the one in hydrogen.

1 Introduction

During the current transition towards renewable energy sources, the demand for versatile devices able to store and re-use the excess of energy production is increasing [1–4]. In this scenario, Solid Oxide Fuel Cells (SOFCs) exhibit tempting features, such as high efficiency and low environmental impact [5–8].

Although hydrogen is the most conventional and studied fuel for this application, ammonia is constantly gaining more attention as alternative [9–14]. Ammonia is mainly synthetized though Haber-Bosch method , however more environmentally friendly routes are under investigation [15,16]. Ammonia is largely used in household cleaning products, fertilizers and nitric acid production [17]. It does not present severe safety concerns: it is toxic but human nose is sensible below a concentration of 1 ppm so the detection of leakage is easy [9]. In addition, ammonia has a narrower combustion range than hydrogen [14]. All these features promote the ammonia as an interesting hydrogen carrier and then it deserves a deeper study in SOFC technology.

In 1980, Farr and Vayenas [18] investigated the odds to synthetize NO and obtaining an electrical current during the same process. In the early 2000s, Wojcik and co-workers [19] explored the use of ammonia as fuel to feed a SOFC and they collected promising results.

It has been proposed a two-step mechanism when anode is fed by ammonia in oxygen anion conducting SOFC: first ammonia cracks in nitrogen and hydrogen via thermal decomposition mediated by a catalyst. Then the hydrogen diffuses across the interface reacting with the oxygen to form water [12]. Ni cermet, such as Ni-Yttria Stabilized Zirconia (YSZ) and Ni-Gadolinium Doped Ceria (GDC), have been largely studied for running SOFC on ammonia as fuel [20–23].

Hereby, we propose Ni and La co-doped strontium titanate as anode material. We already investigated $SrTiO_3$ – based materials showing interesting properties for this application [24]. In the current work, we try to impart new functionalities using the method of the exsolution [25–29]. It has been recently employed for anode application in SOFC technology and it allows to realize high dispersive nanoparticles on the surface of the catalyst for preventing drawbacks connected to sintering in long-term operation [30,31].

Ni exsolution in titanates – based materials have been studied as alternative to state-of-art Ni-YSZ for working as anode in high temperature SOFC [27,32,33]. Lanthanum aims to promote the formation of the redox couple of the titanium Ti (IV)/ Ti (III) [34].

In this contribution, we focus our attention on the response of La and Ni co-doped titanates towards ammonia decomposition. The material demonstrates suitable features in reducing environment under operation condition preserving the perovskite structure, as H_2 – Temperature Programmed Reduction (TPR) establish. Catalytic tests prove a totally conversion of ammonia at working temperature (800°C), although the whole decomposition, in nitrogen and hydrogen, occurs at 720°C. From the measurements Ni exsolved nanoparticles do not affect the catalytic activity towards the ammonia cracking. Instead, Ni nanoparticles strongly boost the electrochemical performances, as detected in

impedance measurements at 800°C. To increase furtherly the temperature would enhance the cell tests; for this reason, other tests are under investigation.

2 Experimental

2.1 Synthesis

Regarding the synthesis of $La_{0.45}Sr_{0.45}Ti_{0.90}Ni_{0.10}O_3$, (LSTNO) stoichiometric amounts of La_2O_3 (Sigma-Aldrich, 99.9%) $SrCO_3$ (Sigma-Aldrich, 98%), $C_{12}H_{28}O_4Ti$ (Sigma-Aldrich, 97.0%) and $Ni(NO_3)_2{\cdot}6H_2O$ (Sigma-Aldrich, 97.0%) were dissolved in distilled water and nitric acid under continuous heating and stirring. Precursor's solutions were added to a solution of citric acid; precursors/citric acid ratio is 1/1.8. Subsequently, ammonium hydroxide was added to adjust the pH between 7 and 8. The solution was heated and stirred at 80°C to permit the solvent evaporation and then left to age for 24 hours. Self-combustion was ignited increasing the temperature above 300°C. The ashes-like material was then grinded and calcined at 1000°C for 12 hours (rate 6°C min^{-1}). $La_{0.45}Sr_{0.45}TiO_3$ (LSTO) was synthetized using the same method. The calcined $La_{0.45}Sr_{0.45}Ti_{0.90}Ni_{0.10}O_3$ was treated in 5% H_2/Ar flow to promote the exsolution at 900°C for 20 hours (rate 7°C min^{-1}), as reported in [27]. After the reducing treatment, material has been named $La_{0.45}Sr_{0.45}Ti_{0.90}Ni_{0.10-\delta}O_3$ (LSTNOH).

2.2 Characterization

Crystalline structure of the powders was characterized by X-Ray Diffraction (XRD) using a Brucker D8 Advance diffractometer with Bragg-Brentano geometry and Cu Kα radiation (40 kV, 40 mA, λ = 1,54 Å). H_2 - Temperature Programmed Reduction measurements were carried out through an Autochem II 2920 Micromeritics equipped with a thermal conductivity detector (TCD). H_2 – TRP measurements were led in a quartz tube with 50 mg of the sample powder. The heating goes from room temperature (RT) to 900°C at 10°C/min under a constant flow of 5 vol% H_2/Ar and a flow rate of 50 sccm.

2.3 Catalytic measurements

The sample powder (50 mg) was loaded in quartz tube reactor of 6 mm internal diameter and was exposed to a flow of 10 vol% NH_3/Ar balance helium (He is also the gas carrier). All gas flows were monitored by a thermal mass flow meter and the total inlet flow is 100 sccm. Analysis were performed from RT to 800°C. Samples were pre-treated in He for 1 hour at 100°C before the measurements. The composition of the outlet gas was measured with an Agilent 7890 A gas chromatograph equipped with a TCD and two columns (molecular sieve 13X, 60/80 mesh, 1.8; Porapak Q, 1.8 m). Calibration was carried out using standard gases containing known concentration of the components. NH_3 conversion yield was calculated as reported in [22], F indicates the fraction of fuel (ammonia, 10% in this work) in the flow:

$$NH_3 \text{ conversion yield (\%)} = [(F\ NH_3 \text{ inlet} - F\ NH_3 \text{ unreacted}) / F\ NH_3 \text{ inlet}] * 100 \quad (1)$$

2.4 Cell manufacturing and measurements

The electrochemical tests were carried out on symmetric button cell. Thick electrolyte was prepared by pressing a commercial 8 mol% Yttria-stabilized Zirconia (8YSZ) powder (Fuel Cell Materials) in to pellet and fired in air. Symmetric electrodes were deposited a homemade screen-printing machine and then fired in air at 1200°C for 2 hours. Final circular electrodes have an area of 1,13 cm^2. Electrodes are composite made up by the anodic material and 8YSZ (50:50). Ink preparation involved mixing the powders with a proper amount of binder to adjust the viscosity and 3 wt% of carbon soot to guarantee the porosity to the electrodes. Gold paste was deposited as electron collector and treated at 800°C. Symmetric cell tests were carried out in a home-made single chamber set up using a flow rate of 100 sccm. Electrochemical Impedance Spectroscopy (EIS) measurements were performed through an Autolab Frequency Response Analyser in a frequency range of 10^{-2} – 10^{-6} Hz. The values of area specific resistance (ASR) were calculated considering one electrode in the symmetric cell and its surface area (1.13 cm^2), starting from polarization resistance (R_p) values obtained from impedance measurements.

3 Characterization

3.1 XRD

XRD analysis were performed at room temperature. Diffractograms are displayed in Fig. 1. La – doped $SrTiO_3$, LSTO, shows the characteristic reflections of perovskite crystal structure. The structure is also maintained when Ni is added. Moreover, it has been likely incorporated in the lattice because no further phases appear in the diffractogram. It suggests that 10 mol% of Ni is completely soluble in $La_{0.45}Sr_{0.45}TiO_3$. The insertion in Fig. 1 exhibits an enlargement of the reflection at ~ 46.5° (2θ) The diffractograms in samples containing nickel, LSTNO and LSTNOH, are shifted towards lower angle respect to LSTO. Here, this shift in normally attributed to the substitution of Ti^{4+} atoms, 61 pm, with those larger of Ni^{2+}, 69 pm [35]. This effect indicate that the Ni atoms have been successfully merged in the perovskite lattice producing a consequent expansion of the unit cell [27,36].
Reducing treatment for the exsolution, 900°C for 20 hours in 5% H_2/Ar, causes the release of Ni atoms which move towards the surface forming metal nanoparticles. The reflections in LSTNOH diffractograms demonstrate that the perovskite has been preserved and Ni phase

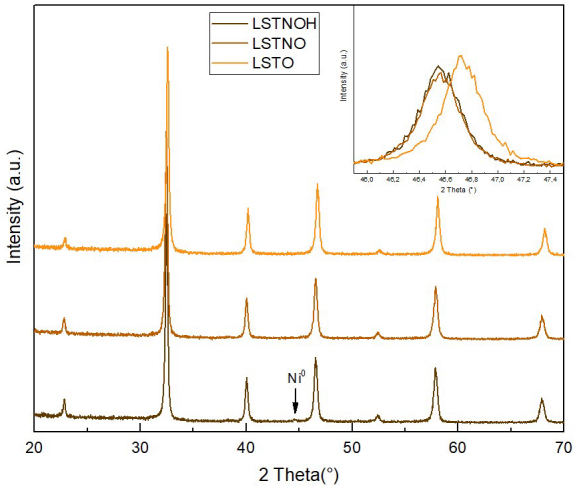

Fig. 1: room temperature XRD of $La_{0.45}Sr_{0.45}TiO_3$ and $La_{0.45}Sr_{0.45}Ti_{0.90}Ni_{0.10}O_3$ calcination at 1000°C in air (LSTO and LSTNO, respectively); LSTNO was furtherly treated at 900°C for 20 h in 5% H_2/Ar: $La_{0.45}Sr_{0.45}Ti_{0.90}Ni_{0.10-\delta}O_3$ (LSTNOH). Insertion: closer inspection of reflection at ~ 46.6° (2θ).

appears at ~ 44.5° (2θ), the most intense reflection, as identified from JCPDS database (# 96-901-3025).

3.2 H_2 – TPR

All TPR measurements were carried out in 5% H_2/Ar from room temperature to 900°C with a ramp of 10°C/minute. Moreover, for LSTNOH sample, a pre – treatment in He at 300°C for 1 hour was also carried out before the TPR analysis in order to remove molecules eventually adsorbed after the exposition with the air, as suggested from the literature [37]. However, it is not reported in Fig. 2 because no variations in the profile have been detected. All TPR profiles are displayed in Fig. 2 (all detectable signals occur between 250 – 750°C). It is well-known that titanate-based materials show high stability in reducing environment, this the reason why they are largely studied for anode application in fuel cells. Indeed, literature works attribute a slightly consumption of hydrogen in LSTO to the reduction from Ti^{4+} to Ti^{3+} [38]. However, in this current work, it is really difficult to distinguish the hydrogen consumption and the background noise because the signal is very low and no well-defined peaks appear. Some considerations can be achieved: in the TPR profile of LSTNO, the peak at ~ 475°C can be associated to the reduction of different nickel oxide species. In particular this signal can be ascribed to surface NiO that might had not been fully incorporated in the perovskite structure [37,39,40]. LSTNO might be exploited to achieve information for the exsolution. Since the condition for this process are stronger (900°C for 20 hours), in the current case, the TPR profile is not diagnostic for this process because there is not any clear variation in the TCD signal. Analysing LSTNOH, two peaks at ~ 375°C and 530°C might correspond to the reduction of nickel oxide state, different to those in LSTNO [40]. No deeper investigations were carried out to identify the phases.

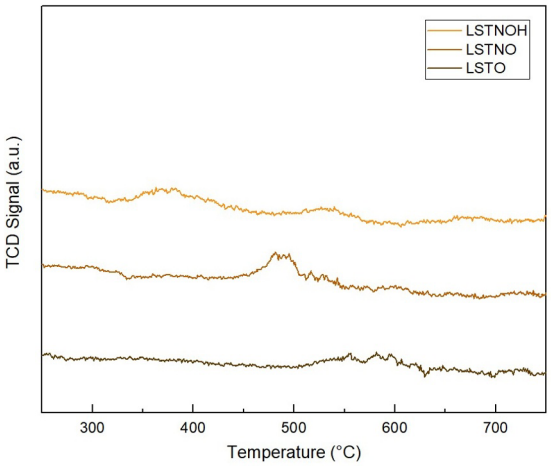

Fig. 2: H_2 - TPR curves obtained for the samples: the $La_{0.45}Sr_{0.45}TiO_3$ (LSTO), $La_{0.45}Sr_{0.45}Ti_{0.90}Ni_{0.10}O_3$ (LSTNO) and $La_{0.45}Sr_{0.45}Ti_{0.90}Ni_{0.10-\delta}O_3$ (LSTNOH); all profile were reported from 250 to 750°C.

4 Catalytic tests

Catalytic tests were carried out though a Gas Chromatograph with aim to evaluate the conversion yield of the inlet ammonia (10%) in nitrogen and hydrogen. Conversion yield was calculated using Eq. (1), as reported in the Experimental section (2.3). In Fig. 3 the results of the catalytic tests are displayed. Observing the conversion curves, both powders show a really close activity towards ammonia decomposition. In particular, ammonia starts to crack at 560°C and it is completely decomposed at 720°C. In this case, Ni nanoparticles do not affect the reaction yield. Ammonia decomposition tests were led by Song *et al.* [41]. They evaluate the catalytic activity of infiltrated Ni, Co and NiCo doped lanthanum strontium titanate on Samarium Doped Ceria (SDC) scaffold. They highlight how the NiCo alloy nanoparticles shows the superior conversion (95,3% at 800°C), while pure SDC scaffold exhibits the lowest, 5,8% at 800°C. This demonstrate that electrolyte oxides show really poor catalytic activity, it must be imparted by the anodic material. However, Molouk and co-workers [22] study the ammonia decomposition on Ni-YSZ and Ni-GDC.
They evidence that Ni-GDC, thanks to a larger number of basic sites on GDC, has higher catalytic activity compared to Ni-YSZ. The choice of the electrolyte affects the ammonia conversion yield.

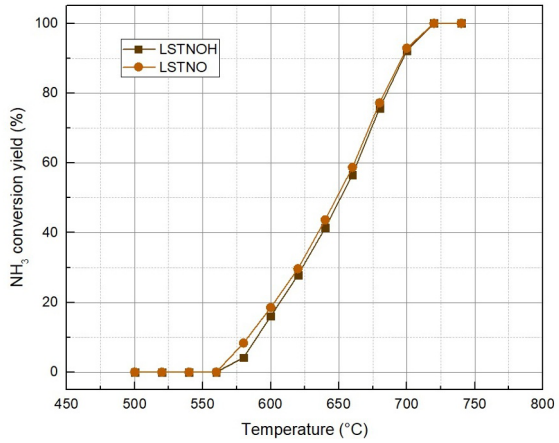

Fig. 3: NH_3 conversion yield as a function of the temperature. Ammonia content in the flow (100 sccm) was 10%.

5 Electrochemical tests

Electrochemical investigations were carried out at 800°C on LSTO, LSTNO and LSTNOH. They were studied forming a composite with 8YSZ (50:50) with the purpose to provide ionic conductivity to the electrode [24]. In Fig. 4 impedance spectra are displayed using 10% NH_3/Ar as fuel. Hydrogen is reported for comparison. Spectra were analysed by mean the method of equivalent circuit. In literature, the most used model circuit [33,42] is made up by a resistor R_1, which refers the resistance of the electrolyte, and then two resistor-constant phase elements (R-CPE) in series to describe the semicircles at high frequency (~ 10^4 - 10^3) and medium frequency (~ 10 – 1 Hz) region. There are no further processes when the cell works with ammonia instead of hydrogen, although the ammonia oxidation involves two steps. The process in high frequency region may be attributed to a not perfect adhesion at the interface between the electrode and electrolyte [42]. Decreasing the amount of soot in order to diminish the porosity may improve the goodness of the interface. Another solution could be a buffer layer between the electrode and the electrolyte with the aim to increase the ion diffusion. However, the main contribute to the total resistance derives from the second process [33]. It could be assigned to the reduction and oxidation cycles of the couple Ti (IV)/Ti (III), which governs the electrical conductivity in the material. The resistance would decrease raising the operation temperature [32,34].
In Table 1, all tested cells are reported highlighting their composition and summing up the performances. From the values of polarization resistance is clearly visible that Ni nanoparticles on the surface, in LSTNOH, strongly improve the electrochemical performances. This consideration is valid both when ammonia and hydrogen have been used as fuel. However, considering the catalytic results discussed above, the behaviour of LSTNO and LSTNOH are totally overlapped. In the light of these results, the Ni nanoparticles boost the performance of the electrode: they are more active towards hydrogen oxidation rather than the ammonia decomposition, where the conversion is not affected by Ni nanoparticles. Although, the completely decomposition of ammonia make possible to study the cell performance at lower temperature, likely the cell performance will be worse because titanate-based materials assume high temperature for operation.

Table 1: cell measurements are sum up and cell composition is highlighted. * Polarization resistance values were collected using EIS.

Symmetric cell	% fuel (in Ar)	Rp (Ω)*	ASR (Ω cm²)
LSTNOH+8YSZ (50:50) | 8YSZ	10 H_2	22,6	12,8
LSTNOH+8YSZ (50:50) | 8YSZ	10 NH_3	24,2	13,7
LSTNO+8YSZ (50:50) | 8YSZ	10 NH_3	79,1	44,7
LSTO+8YSZ (50:50) | 8YSZ	10 NH_3	126,2	71,4

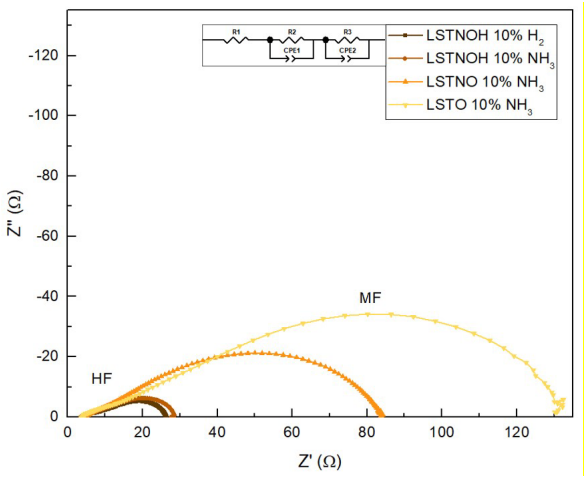

Fig. 4: EIS spectra for the anode composite materials at 800°C using NH_3 (in Ar). Also 10% of H_2 in Ar is reported as reference. The model circuit used for the fitting is displayed.

6 Conclusions

In this contribution we synthetized La and Ni co-doped strontium titanate by means wet chemistry route, a robust and suitable potential anode for SOFC technology. Ni has been exsolved from the perovskite crystal structure through a reducing treatment forming metallic nickel nanoparticles on the surface, as shown in XRD diffractograms. We focused the work on ammonia as alternative fuel. The catalytic behaviour of the material was evaluated by tests measuring the ammonia conversion. LSTNO and LSTNOH exhibit a really close activity. They start to decompose the ammonia at 520°C and the conversion reaches the full yield at 720°C. Instead, LSTNOH shows superior results during electrochemical measurements at 800°C, both in ammonia and hydrogen. Increasing temperature would

diminish the polarization resistance. In the light of these results, ammonia demonstrates interesting properties and deserves a deep investigation, for example using high working temperature. Further work is in progress in order to collect more data in electrochemical measurements. Complete cell tests will be early carried out for measuring the density power and to have clearer the potential of ammonia to feed SOFC.

7 References

[1] M.S. Dresselhaus, I.L. Thomas, Nature **414** (2001) 332–337.

[2] A.M. Abdalla, S. Hossain, A.T. Azad, P.M.I. Petra, F. Begum, S.G. Eriksson, A.K. Azad, Renew. Sustain. Energy Rev. **82** (2018) 353–368.

[3] F. Nadeem, S.M.S. Hussain, P.K. Tiwari, A.K. Goswami, T.S. Ustun, IEEE Access **7** (2019) 4555–4585.

[4] A.G. Olabi, C. Onumaegbu, T. Wilberforce, M. Ramadan, M.A. Abdelkareem, A.H. Al – Alami, Energy **214** (2021) 118987.

[5] S.C. Singhal, Solid State Ionics **135** (2000) 305–313.

[6] N. Mahato, A. Banerjee, A. Gupta, S. Omar, K. Balani, Prog. Mater. Sci. **72** (2015) 141–337.

[7] M. Mehrpooya, M. Sadeghzadeh, A. Rahimi, M. Pouriman, Energy Convers. Manag. **198** (2019) 111767.

[8] A.B. Stambouli, E. Traversa, Renew. Sustain. Energy Rev. **6** (2002) 433–455.

[9] A. Fuerte, R.X. Valenzuela, M.J. Escudero, L. Daza, J. Power Sources **192** (2009) 170–174.

[10] M. Ni, M.K.H. Leung, D.Y.C. Leung, Int. J. Hydrogen Energy **33** (2009) 943–959.

[11] A. Valera-medina, H. Xiao, M. Owen-Jones, W.I.F. David, P.J. Bowen, Prog. Energy Combust. Sci. **69** (2018) 63–102.

[12] O. Siddiqui, I. Dincer, Therm. Sci. Eng. Progess **5** (2018) 568–578.

[13] Q. Ma, R.R. Peng, L. Tian, G. Meng, Electrochem. Commun. **8** (2006) 1791–1795.

[14] G. Jeerh, M. Zhang, S. Tao, J. Mater. Chem. A **9** (2021) 727–752.

[15] E. Morgan, J. Manwell, J. McGowan, Renew. Energy **72** (2014) 51–61.

[16] C. Smith, A.K. Hill, L. Torrente-Murciano, Energy Environ. Sci. **13** (2020) 331–344.

[17] T.E. Bell, L. Torrente-Murciano, Top. Catal. **59** (2016) 1438–1457.

[18] R.D. Farr, C.G. Vayenas, Energy Dev. Japan **4** (1981) 111–128.

[19] A. Wojcik, H. Middleton, I. Damopoulos, J. Van herle, J. Power Sources **118** (2003) 342–348.

[20] G.G.M. Fournier, I.W. Cumming, K. Hellgardt, J. Power Sources **162** (2006) 198–206.

[21] Q. Ma, J. Ma, S. Zhou, R. Yan, J. Gao, G. Meng, J. Power Sources **164** (2007) 86–89.

[22] A.F.S. Molouk, J. Yang, T. Okanishi, H. Muroyama, T. Matsui, K. Eguchi, J. Power Sources **305** (2016) 72–79.

[23] J. Yang, A.F.S. Molouk, T. Okanishi, H. Muroyama, T. Matsui, K. Eguchi, ACS Appl. Mater. Interfaces **7** (2015) 28701–28707.

[24] G. Carollo, A. Garbujo, F. Mauvy, A. Glisenti, Energy and Fuels **34** (2020) 11438–11448.

[25] D. Neagu, G. Tsekouras, D.N. Miller, H. Ménard, J.T.S. Irvine, Nat. Chem. **5** (2013) 916–923.

[26] D. Neagu, T.S. Oh, D.N. Miller, H. Ménard, S.M. Bukhari, S.R. Gamble, R.J. Gorte, J.M. Vohs, J.T.S. Irvine, Nat. Commun. **6** (2015) 1–8.

[27] G. Tsekouras, D. Neagu, J.T.S. Irvine, Energy Environ. Sci. **6** (2013) 256–266.

[28] B.A. Rosen, Electrochem **1** (2020) 32–43.

[29] D. Neagu, E.I. Papaioannou, W.K.W. Ramli, D.N. Miller, B.J. Murdoch, H. Ménard, A. Umar, A.J. Barlow, P.J. Cumpson, J.T.S. Irvine, I.S. Metcalfe, Nat. Commun. **8** (2017) 1–8.

[30] K. Kousi, C. Tang, I.S. Metcalfe, D. Neagu, Small **17** (2021) 2006479.

[31] J.T.S. Irvine, D. Neagu, M.C. Verbraeken, C. Chatzichristodoulou, C. Graves, M.B. Mogensen, Nat. Energy **1** (2016) 1–13.

[32] D. Neagu, J.T.S. Irvine, Chem. Mater. **22** (2010) 5042–5053.

[33] D.N. Miller, J.T.S. Irvine, J. Power Sources **196** (2011) 7323–7327.

[34] O.A. Marina, N.L. Canfield, J.W. Stevenson, Solid State Ionics **149** (2002) 21–28.

[35] B.H. Park, G.M. Choi, Solid State Ionics **262** (2014) 345–348.

[36] B.H. Park, G.M. Choi, J. Power Sources **293** (2015) 684–691.

[37] M. Toscani, F. Volpe, N. Nichio, Int. J. Hydrogen Energy **5** (2020) 23433–23443.

[38] J. Li, T. Lv, N. Hou, P. Li, X. Yao, L. Fan, T. Gan, Y. Zhao, Y. Li, Int. J. Hydrogen Energy **42** (2017) 22294–22301.

[39] J. Marrero-Jerez, E. Chinarro, B. Moreno, M.T. Colomer, J.R. Jurado, P. Núñez, Ceram. Int. **40** (2014) 3469–3475.

[40] A. Mizera, E. Drożdż, Ceram. Int. **46** (2020) 24635–24641.

[41] Y. Song, H. Li, M. Xu, G. Yang, W. Wang, R. Ran, W. Zhou, Z. Shao, Small **16** (2020) 1–8.

[42] C. Arrivé, T. Delahaye, O. Joubert, G. Gauthier, J. Power Sources **223** (2013) 341–348.